Empirical potential-based Si-Ge interatomic potential and its application to superlattice stability

Tomonori Ito, K. E. Khor, and S. Das Sarma
Department of Physics and Astronomy, University of Maryland, College Park, Maryland 20742-4111
(Received 6 April 1989)

A new empirical interatomic potential for Si-Ge alloy system is proposed based on the Khor–Das Sarma universal interatomic potential for tetrahedrally bonded materials. We modify the Khor–Das Sarma potential and check its validity by calculating the elastic constants of Si and Ge using the homogeneous-deformation method. The feasibility for applying this potential to binary systems is tested by investigating pressure-induced phase transitions associated with isotropic compression and tetragonal distortion. The new empirical potentials for Si, Ge, and Si-Ge are used to calculate thermodynamic properties such as lattice parameters, bond lengths, and excess energies for Si-Ge superlattices. The calculated results are shown to be in good agreement with available experimental data. We also calculate the phonon dispersion for bulk Si. The newly obtained empirical potentials for Si, Ge, and Si-Ge should be useful for investigating Si-Ge binary systems.

I. INTRODUCTION

Empirical interatomic potentials for Si have been extensively used for investigating many aspects of semiconductor properties such as microcluster formation,[1,2] amorphous structure formation,[3,4] epitaxial growth,[5,6] and surface reconstructions.[7] Although attempts at constructing such a potential for specific applications have met with some success, most of the empirical potentials used in these studies fail to predict correctly the relative stability of various structures and give quantitatively wrong results even for simple elastic constants.

Khor and Das Sarma[8] have proposed universal interatomic potentials for elemental semiconductors based on the idea that bonding energies of many substances can be modeled by pairwise interactions. The interatomic potentials for C, Si, and Ge provided a global fit to cohesive energies for various structures. Furthermore, using this Si interatomic potential, reconstructions on the Si(100) and Si(111) surface have been studied. The calculated results are in good agreement with experiment and *ab initio* total-energy calculations.[9,10] These results imply that the Khor–Das Sarma potential gives the right order of stability for various atomic configurations with large bond-angle distortions, which is one of the more important criteria for applying the interatomic potential to binary systems.

In this paper, we propose a new interatomic potential for a binary system of elemental semiconductors based on the Khor–Das Sarma potential. The new potential is obtained by modifying the bond-bending term to calculate the elastic constants for Si and Ge using the homogeneous-deformation method. To check the feasibility of applying the modified potentials for Si and Ge to the binary system, a pressure-induced phase transition with respect to isotropic compression and tetragonal distortion are investigated. In particular, energy changes as functions of atomic volume and axial ratio are calculated and discussed. Finally, the modified potential is applied to the Si-Ge superlattices such as Si_3Ge_1 and Si_1Ge_3 using Si, Ge, and the newly determined Si-Ge interatomic potentials. The versatility of these interatomic potentials is established by calculating equilibrium states of these superlattices.

II. POTENTIAL MODIFICATION AND ELASTIC CONSTANTS FOR Si AND Ge

Cowley[11] pointed out that none of the empirical potentials, which have been proposed by Stillinger and Weber,[12] Tersoff,[13] and Biswas and Hamann,[14] is completely satisfactory in the calculation of elastic constants, in spite of their success in describing structural properties. This indicates that the calculation of elastic constants is a severe test for the reliability of interatomic potentials.

Elastic constants can be determined using either of the following two methods. One is a static treatment, i.e., the homogeneous deformation method, where ions are located on the lattice points within the adiabatic approximation. The other is a dynamical treatment, i.e., long-wave phonon velocity method, where ions are displaced around the lattice points. It was shown by Wallace[15] that, in general, calculations of elastic constants using these two methods are essentially equivalent. For simplicity, we employ the homogeneous deformation method.

The independent elastic constants of cubic crystals are given by considering the following homogeneous deformations.[16] Assuming uniform volume expansion denoted by $R_x'=v^{1/3}R_x$, $R_y'=v^{1/3}R_y$, and $R_z'=v^{1/3}R_z$, where R is the lattice point, the bulk modulus $B=(c_{11}+2c_{12})/3$ is given by

$$B=\frac{1}{\Omega}\frac{d^2E_{\rm coh}}{dv^2}\ , \tag{1}$$

where $E_{\rm coh}$ is cohesive energy and Ω is atomic volume. Next, considering shear deformation in one plane, denoted by $R_x'=R_x+\gamma_1 R_y$, $R_y'=R_y$, and $R_z'=R_z$, where the crystal volume is taken to remain constant, the shear modulus c_{44} is obtained by

$$c_{44}=\frac{1}{\Omega}\frac{d^2E_{\rm coh}}{d\gamma_1^2}\ . \tag{2}$$

Third, considering compression in one direction, denoted by $R_x'=(1+\epsilon_1)R_x$, $R_y'=R_y/(1+\epsilon_1)$, and $R_z'=R_z$, where the crystal volume is also maintained constant, the shear modulus $C'=(c_{11}-c_{12})/2$ is defined by

$$C'=\frac{1}{4\Omega}\frac{d^2E_{\rm coh}}{d\epsilon_1^2}\ . \tag{3}$$

Cohesive energy $E_{\rm coh}$ is obtained from the interatomic potential V_{ij} proposed by Khor and Das Sarma:[8]

$$E_{\rm coh}=\tfrac{1}{2}\sum_{\substack{i,j\\(i\neq j)}}V_{ij}\ , \tag{4}$$

$$V_{ij}=Ae^{-\beta(r_{ij}-R_i)^\gamma}\left[e^{-\theta r_{ij}}-B_0e^{-\lambda r_{ij}}\frac{G(\theta)}{Z_i^\alpha}\right]\ , \tag{5}$$

$$G(\theta)=1+\sum_{k\ (\neq i,j)}[\cos(\eta\,\Delta\theta_{jik})-1]\ . \tag{6}$$

Here, r_{ij} is the interatomic distance between an atom i and a neighbor j,

$$Z_i=\sum_{ij}\exp[-\beta(r_{ij}-R_i)^\gamma]$$

gives the effective coordination number of atom i, R_i is the minimum interatomic distance of its neighbors, η is the bond-bending constant, $\Delta\theta_{jik}=\theta_{jik}-\theta_i$, θ_i is an equilibrium bond angle, and θ_{jik} is the angle between ij and jk.

According to the valence-force-field (VFF) approach,[17,18] the distortion energy corresponding to bond bending is recognized to consist of two contributions of $(\Delta\theta)^2$ and $(\Delta\theta\,\Delta r)$. However, the contribution of $(\Delta\theta\,\Delta r)$, which might be particularly important in the calculation of c_{44} with respect to both changes of bond angle and bond length, is not taken into account in $G(\theta)$. The function $G(\theta)$ is modified without adding further parameters by introducing the $(\Delta\theta\,\Delta r)$ term based on VFF model as

$$G(\theta)=1+\sum_{k\ (\neq i,j)}\left[\cos(\eta\Delta\theta_{jik})-1-\left[\frac{\eta}{2\sqrt{2}}\frac{\Delta r_{ij}}{r_e}\right]\times\sin(\Delta\theta_{jik})\right]\ ,$$

$$\Delta r_{ij}=r_{ij}-r_e\ , \tag{7}$$

$$r_e=\frac{1}{\theta-\lambda}\left[\alpha\ln(Z_i)+\ln\left[\frac{\theta-\lambda}{B_0}\right]\right]\ .$$

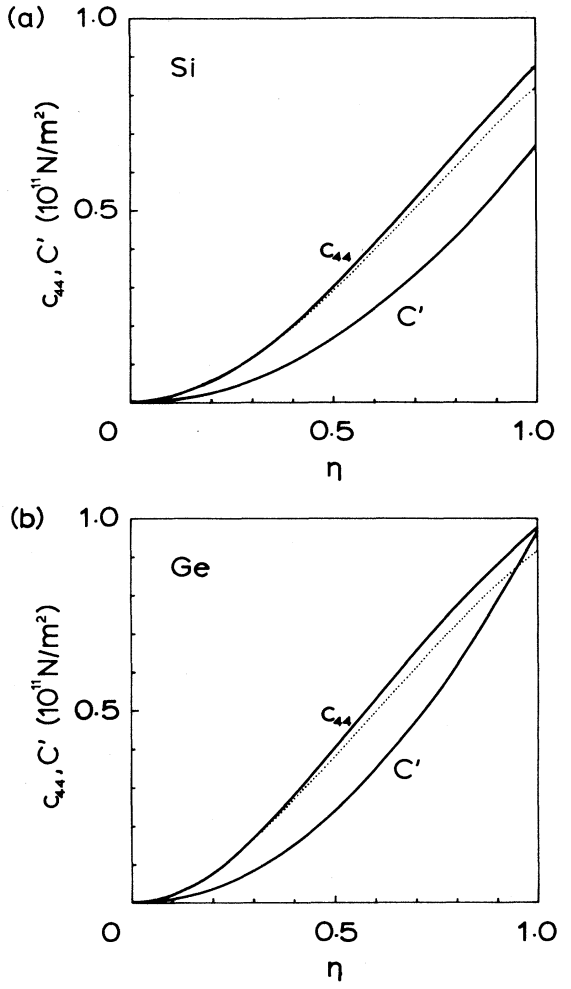

FIG. 1. Calculated elastic constants of c_{44} and C' for Si (a) and Ge (b) as a function of η. Solid and dotted lines for c_{44} correspond to the results using modified and previous interatomic potentials.

The potential parameters A, B_0, θ, λ, α, β, and γ are determined using our method previously reported.[8] The elastic constants c_{44} and C' can be obtained as a function of η using these potential parameters. Figures 1(a) and 1(b) show the values obtained for c_{44} and C' for Si and Ge, respectively, based on the modified interatomic potentials defined by Eqs. (5) and (7). They are compared with the c_{44} results obtained by the previous interatomic potential (dotted line). It is clear that the modified potential gives a larger c_{44} than the previous potential because of the contribution of $(\Delta r\,\Delta\theta)$ term. The differences between c_{44} estimated from modified and previous poten-

TABLE I. The values of potential parameters in Eq. (7) for Si and Ge.

	A (eV)	B_0	θ (Å^{-1})	λ (Å^{-1})	α	β	γ	η
Si	2794.2386	0.082 517 16	3.132 69	1.341 46	0.624 909 6	25.441 23	3.382 18	0.893 711
Ge	1498.7626	0.383 766 4	2.372 39	1.631 05	0.342 635 1	17.798 61	3.228 77	0.670 128

TABLE II. Elastic constants and those pressure derivatives at atmospheric pressure, SW, T, and BH denote the results for Stillinger-Weber, Tersoff, and Biswas-Hamann potentials, respectively (Ref. 11). Elastic constants are in units of 10^{11} N/m^2.

	Si					Ge	
	SW	T	BH	This work	Expt.	This work	Expt.
c_{11}	1.514	1.044	1.71	1.689	1.657	1.346	1.289
c_{12}	0.764	0.597	1.00	0.626	0.639	0.481	0.483
c_{44}	0.564	0.390	0.92	0.754	0.796	0.613	0.671
C'	0.375	0.224	0.36	0.531	0.509	0.433	0.403
B	1.014	0.746	1.24	0.981	0.978	0.770	0.752
dc_{44}/dp				0.797	0.80	1.298	1.30
dC'/dp				0.086	0.075	0.272	0.34
dB/dp				3.831	4.24	3.581	4.60

tials are about 5% for Si and 8% for Ge.

The bond-bending constant η is determined to reproduce the pressure derivative dc_{44}/dp at atmospheric pressure, since the pressure derivative is very sensitive to any change in the value of η. The values of the potential parameters and calculated elastic constants for Si and Ge obtained by Eqs. (1), (2), and (3) are listed in Tables I and II, respectively. In Table II, our calculated results are found to be in excellent agreement with the available experimental data.[19,20] This can be compared with the results obtained by Cowley for the other interatomic potentials where the error in c_{44} for Si is in the range of 15%–50%. Therefore, the new interatomic potentials, using the same formulation for Si and Ge, predict not only the correct order of relative stability for various structures but also produce good elastic constants.

The calculated phonon-dispersion curve for Si is shown in Fig. 2, along with the experimental data. Good agreement between theory and experiment for the acoustic branch near the zone center reflects the fact that this interatomic potential predicts correct elastic constants. Our calculated phonon-dispersion results are comparable to the results for the Stillinger-Weber potential, which has been shown to give the best overall description of the lattice dynamics in a comparative study of the empirical potentials of Tersoff, of Stillinger and Weber, and of Biswas and Hamann.[11]

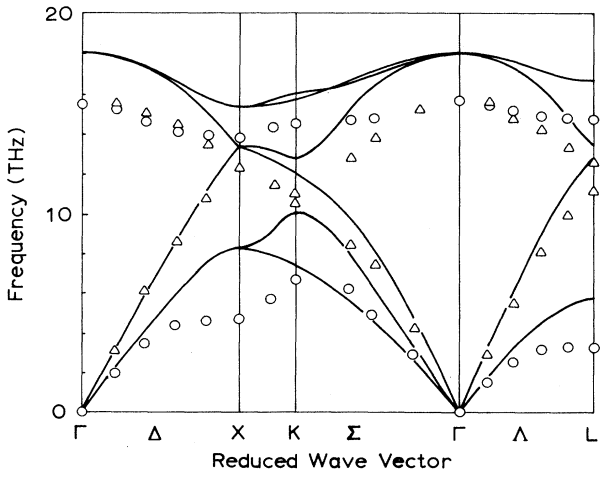

FIG. 2. Calculated phonon-dispersion curves for Si. Open circles and triangles are experimental results.

It is known that the valence-force-field (VFF) model gives the phonon spectra of Si and Ge successfully.[21] Aside from the two primary (bond bending and bond stretching) and one interaction ($\Delta\theta\,\Delta r$ term) force constants we have used here, the VFF model includes three other interaction constants ($\Delta r\,\Delta r'$ and two $\Delta\theta\,\Delta\theta'$ terms). These extra terms can be taken into account in Eqs. (5) and (7) in a natural way; then, in principle, we should be able to reproduce the correct spectra, including the TA flattening.

III. PRESSURE-INDUCED PHASE TRANSITION

Interatomic distances of Si-Si and Ge-Ge in Si-Ge binary systems are known to be different from those in Si and Ge. The equilibrium interatomic distance in disordered $Si_{1-x}Ge_x$ is affected by the change of lattice parameter, which varies with x, and local lattice distortion.[22] The change in interatomic distances induced by tetragonal distortion is also found in the strained layer heterostructure such as $Si_{1-x}Ge_x/Si$.[23] Both the processes of lattice-parameter change and tetragonal distortion occur in pressure-induced phase transition for bulk Si and Ge.

It has been observed experimentally that group-IV elemental semiconductors display covalent(diamond structure)—metallic(β-Sn structure) transition under high pressure.[24,25] This involves isotropic and tetragonal deformations, corresponding, respectively, to the variation of cohesive energy with lattice parameter and axial ratio c/a. Pressure-induced phase transition then is expected to be a good test of the applicability of the new Si and Ge interatomic potentials to Si-Ge binary systems.

In the calculation of the cohesive energy, we note that there are two bond angles in the β-Sn case, where interaction between two bonds with the larger bond-angle does not contribute to the bond-bending energy. For simplicity, we assume this to be the case for $c/a \neq 1$—this seems to be a reasonable assumption if the difference between bond angles is large.

Before discussing pressure-induced phase transition,

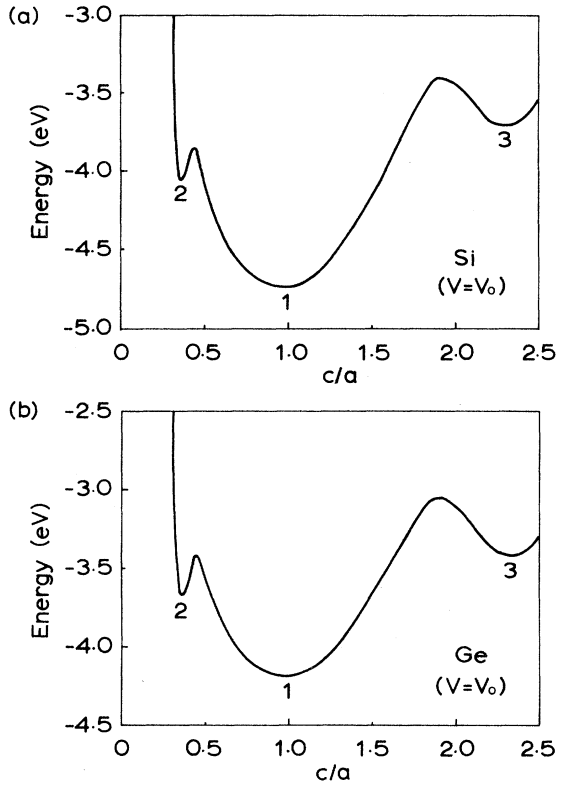

FIG. 3. Calculated cohesive energy change for Si (a) and Ge (b) as a function of axial ratio c/a. The calculation is performed at equilibrium atomic volume $V=V_0$ under atmospheric pressure. The cubic cell with axial ratio $c/a=1$ is taken as a unit cell for diamond structure in this study.

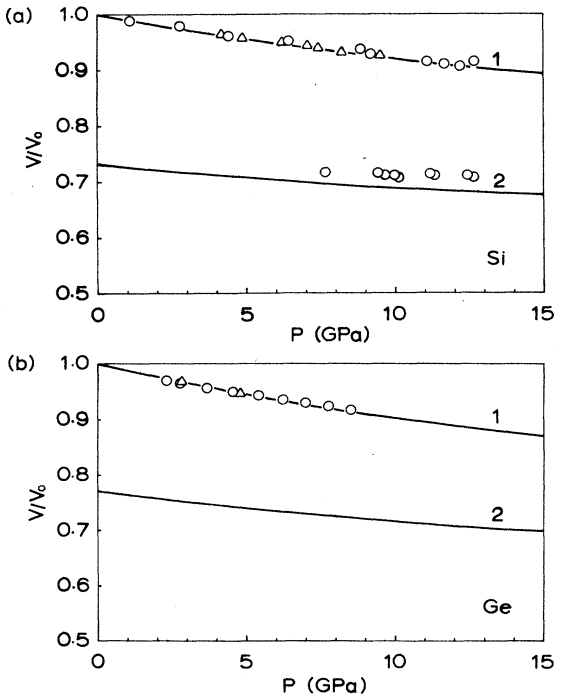

FIG. 4. Calculated pressure-volume relationship for Si (a) and Ge (b) with diamond ("1") and β-Sn(I) ("2") structures. Open circles and triangles are the experimental results.

we display the behavior of the calculated energy as a function of the axial ratio c/a at equilibrium atomic volume V_0 for Si and Ge in Figs. 3(a) and 3(b), respectively. As can be clearly seen, there are three local energy minima in these figures, i.e., the diamond structure (denoted by "1" in the figures) with lowest energy, β-Sn(I) ("2") and β-Sn(II) ("3") structures with higher energies. The relative stability among these structures is recognized to be reproduced using our new interatomic potentials. However, axial ratio $c/a=0.36$ of β-Sn(I), where the coordination number becomes equal to 6, is slightly

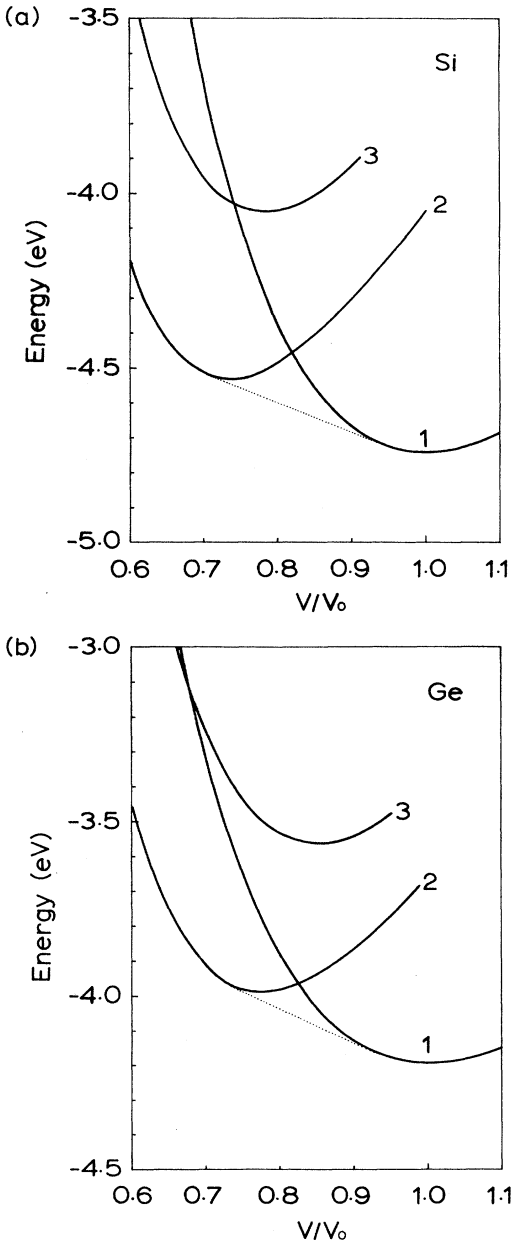

FIG. 5. Calculated cohesive-energy change for Si (a) and Ge (b) with diamond ("1"), β-Sn(I) ("2") and β-Sn(II) ("3") as a function of volume ratio V/V_0. Dotted line denotes the common tangent between diamond and β-Sn(I) structures.

different from the experimental axial ratio $c/a=0.39$.[26] Similar results were obtained in the calculation using Dodson[27] and Tersoff[28] potentials.

The pressure-volume relationships for Si and Ge are shown in Figs. 4(a) and 4(b), respectively. They are compared with experimental results.[29,30] The results agree well with experimental results, quantitatively for diamond and qualitatively for β-Sn(I) structures. The volume-energy relationships for diamond (1), β-Sn(I) (2), and β-Sn(II) (3) in Si and Ge are also shown in Figs. 5(a) and 5(b). These figures suggest that the pressure-induced phase transition only occurs along the common tangent between diamond and β-Sn(I) structures, since the cohesive energies for β-Sn(II) structure are higher than those of β-Sn(I) structure over the entire atomic volume ratio range. This is also consistent with experimental results.

Figures 6(a) and 6(b) show that the energy behavior for Si and Ge as a function of axial ratio c/a near V_t^2, the atomic volume for β-Sn(I) at the phase-transition point. Comparing them with Figs. 3(a) and 3(b), the most stable states are found to change from the diamond structure(1) to the β-Sn(I) structure(2) in both Si and Ge. The diamond-structure state is only an inflection point in these energy curves, which has no activation barrier between diamond and β-Sn(I) structures in contrast to results for Si given by the Dodson and Tersoff potentials as shown in Figs. 7(b) and 7(c), where another metastable state emerges at $c/a=0.52$ because of the activation barrier at $c/a=0.45$. Further, β-Sn(II) structure never appears under high pressure, even if the energy of β-Sn(II) is lower than that of diamond structure in Si, since there is an activation barrier between these structures. It is clear that our potential gives the correct predictions for the pressure-induced phase transitions of Si and Ge. We feel that the new Si and Ge interatomic potentials can be applied to Si-Ge binary systems, which is discussed in the following section.

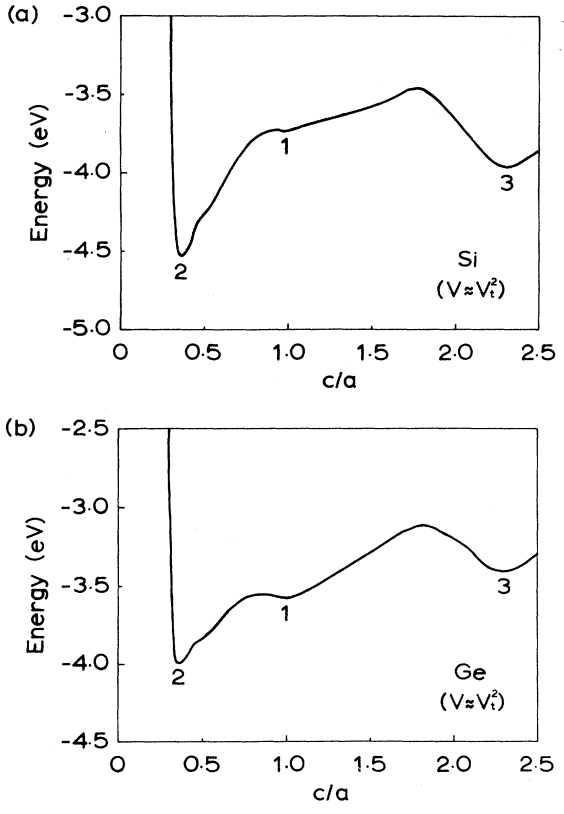

FIG. 6. Calculated cohesive energy change for Si (a) and Ge (b) as a function of axial ratio c/a near phase transition atomic volume $V \simeq V_t^2$.

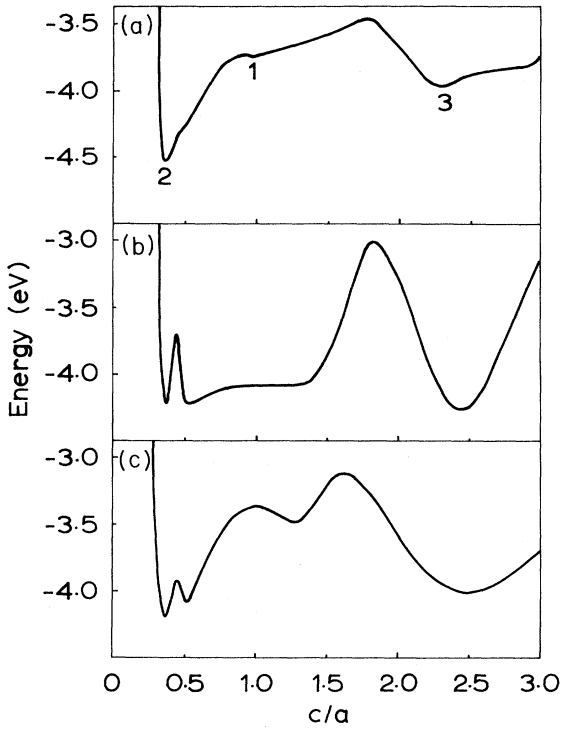

FIG. 7. Comparison of the cohesive energy changes for Si as a function of axial ratio c/a near phase transition atomic volume $V \simeq V_t^2$ using various interatomic potentials. Our calculated result (a) is compared with the results obtained from Dodson (b) and Tersoff (c) potentials.

IV. APPLICATION TO Si-Ge SUPERLATTICES

Si-Ge binary systems including $Si_{1-x}Ge_x$/Si strained-layer heterostructure and superlattice have been subjects of increasing interest in recent years.[31] This is because of their potential for tailoring optoelectronic properties of the materials. In this section, we determine the Si-Ge interatomic potential based on the Si and Ge potentials discussed in Sec. II and attempt the calculation of thermodynamic properties (e.g., lattice parameters, bond lengths, excess energies, and interplanar distances) of Si_3Ge_1, Si_1Ge_3, and Si_2Ge_2 superlattices and the rhombohedral structure using Si, Ge, and Si-Ge interatomic potentials.

TABLE III. The values of potential parameters in Eq. (7) for Si-Ge. η_{SGSS}, η_{SGSG}, and η_{SGGG} denote η for bonds between Si-Ge and Si-Si, Si-Ge and Si-Ge, Si-Ge and Ge-Ge, respectively.

	A (eV)	B_0	θ (Å^{-1})	λ (Å^{-1})	α	β	γ	η_{SGSS}	η_{SGSG}	η_{SGGG}
Si-Ge	1800.4512	0.201 020 4	2.700 09	1.505 21	0.484 562 7	21.981 82	3.313 49	0.847 25	0.794 50	0.735 46

The interatomic potential for Si_1Ge_1 superlattice with zinc-blende structure is determined to satisfy the average values of the lattice parameters, the elastic constants of Si and Ge, and the excess energy to be 10 meV, which is extracted from various first-principles calculations.[32–34] The bond-bending constants η between Si—Si or Ge—Ge and Si—Ge bonds are obtained as interpolated value of Si, Si_1Ge_1, and Ge. The values of potential parameters are summarized in Table III.

The unit cell of Si_3Ge_1, Si_1Ge_1, and Si_1Ge_3 are schematically shown in Fig. 8. To determine the equilibrium structure, the distortion parameter δ and lattice parameter a have been introduced in the energy calculations. There are two assumptions: One is that the axial ratio $c/a=1$, and the other presumes that Ge and Si atoms in Si_3Ge_1 and Si_1Ge_3 superlattices, respectively, are displaced in the (001) direction and the other atoms are located on the regular fcc sublattice.

The minimization of the cohesive energies for Si_3Ge_1 and Si_1Ge_3 superlattices are carried out by varying the parameters a and δ. Figure 9 demonstrates the cohesive energy for Si_1Ge_3 superlattice as a function of the distortion parameter δ. It is found that the energy decreases with distortion and has the lowest value at $\delta=0.016$, which corresponds to the lattice points $(a/4)(1,1,1.016)$ and $(a/4)(1,3,2.984)$ for Ge atoms.

Figure 10 shows the calculated equilibrium lattice parameters for Si-Ge superlattices. The lattice parameters estimated theoretically conform to Vegard's law and are consistent with the experimental results for $Si_{1-x}Ge_x$ (Ref. 35) and *ab initio* pseudopotential calculation for Si-Ge superlattices.[33]

The calculated bond lengths are also shown in Fig. 11. The bimodal distribution of bond lengths, which is induced by the displacement of Si or Ge atoms in the superlattices, can be seen. The calculated results for the bond lengths are slightly different from the experimental results in disordered $Si_{1-x}Ge_x$.[31] However, the discrepancy between the calculated and experimental results does not imply that the calculation has failed to predict the correct bond lengths, since some first-principles calculations have demonstrated that the bond lengths in the superlattice tend to be closer to the model of bond-length conservation than those in the disordered alloy.[36,37]

Figure 12 shows the comparison between the excess energies calculated in this study and those estimated by the regular solution model. It is clear that the behavior of the calculated excess energies as a function of concentration is quite reasonable. *Ab initio* pseudopotential calculations have shown that the rhombohedral structure with *AB-BA* stacking is more stable than the Si_1Ge_1 superlattice.[32,34] The calculated excess energy of the rhombohedral structure is found to be 3 meV lower than that of Si_1Ge_1 superlattice. This is also consistent with the results obtained by *ab initio* pseudopotential calculation.

Further confirmation for the versatility of these interatomic potentials is demonstrated by the calculation of interplanar distances for epitaxial Si_2Ge_2 superlattice grown pseudomorphically on a (001) oriented substrate with lattice parameters of Si, Ge, and the average of Si and Ge. The equilibrium structure of a Si_2Ge_2 superlattice is determined by minimizing its cohesive energy using two variational parameters such as axial ratio c/a and relaxation parameter ϵ, which specify the spacing $d_{\alpha\beta}$ between adjacent planes α and β as $d_{\alpha\beta}=(c/4)(1+\epsilon)$. The calculated interplanar distances are shown in Table IV with the equilibrium axial ratio c/a and relaxation parameter ϵ. Our results are compared with those obtained by the valence force field with *ab initio* parameters.[38] Clearly, the agreement is good, although our interplanar distances are slightly larger. This is because *ab initio* pseudopotential total-energy calculations give smaller equilibrium lattice parameters of Si and

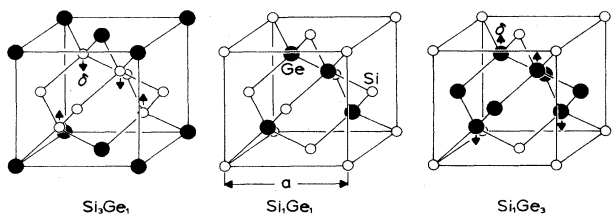

FIG. 8. Unit cell with axial ratio $c/a=1$ for Si_3Ge_1, Si_1Ge_1, and Si_1Ge_3 superlattices used in this study. Lattice parameter a and distortion parameter δ are variational parameters in the superlattice structures.

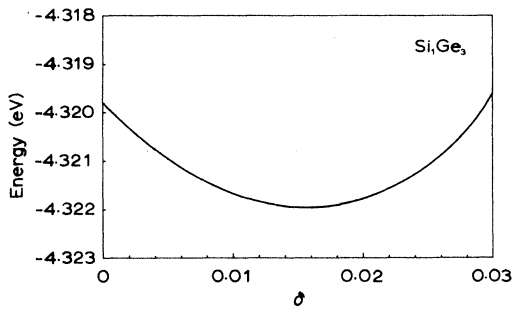

FIG. 9. Calculated cohesive-energy change as a function of the distortion parameter δ in Si_1Ge_3 superlattice.

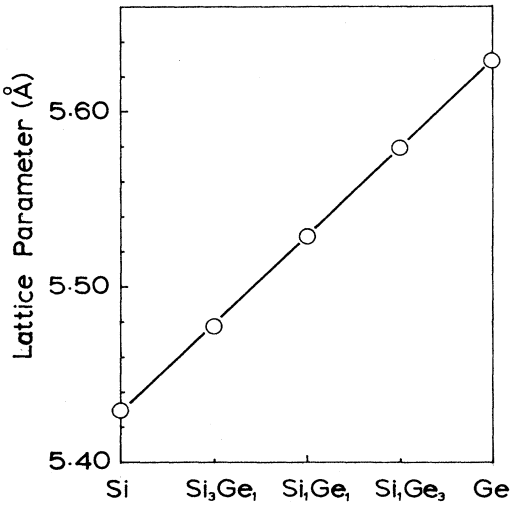

FIG. 10. Calculated lattice parameters for Si-Ge superlattices. Solid line indicates the results conforming to Vegard's law. Si_3Ge_1, Si_1Ge_1, and Si_1Ge_3 are regarded to correspond to $Si_{0.75}Ge_{0.25}$, $Si_{0.5}Ge_{0.5}$ and $Si_{0.25}Ge_{0.75}$, respectively.

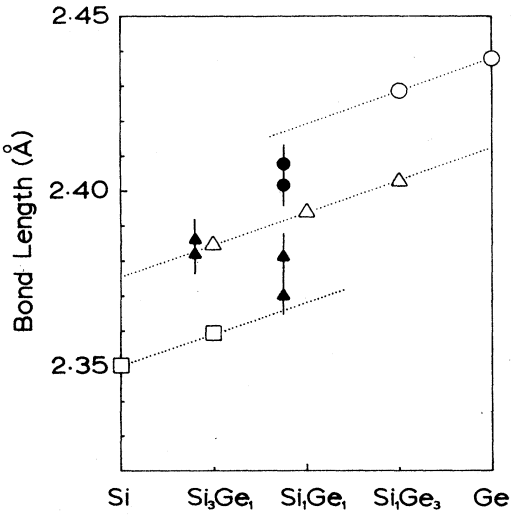

FIG. 11. Calculated bond lengths for Si-Si (open square), Si-Ge (open triangle), and Ge-Ge (open circle) in Si-Ge superlattices. The experimental results for Si-Ge (solid triangle) and Ge-Ge (solid circle) in $Si_{1-x}Ge_x$ are also shown with their error bars.

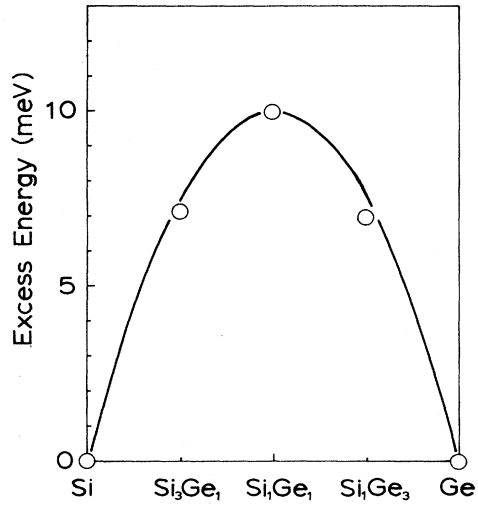

FIG. 12. Calculated excess energies for Si-Ge superlattices. Solid line denotes the results assuming the regular solution model. Si_3Ge_1, Si_1Ge_1, and Si_1Ge_3 are regarded to correspond to $Si_{0.75}Ge_{0.25}$, $Si_{0.5}Ge_{0.5}$, and $Si_{0.25}Ge_{0.75}$, respectively.

Ge than the experimental lattice parameters employed in this study.[8]

These newly derived interatomic potentials for Si, Ge, and Si-Ge have been shown here to give reasonable thermodynamic properties of Si-Ge superlattices. Although the reliability of these potentials should be tested from various viewpoints, these preliminary calculations suggest that the new interatomic potentials are applicable for the thermodynamic study of binary systems consisting of elemental semiconductors.

V. CONCLUSION

We propose new Si and Ge interatomic potentials based on the Khor–Das Sarma potential and check the validity and feasibility of these potentials by studying Si-Ge binary systems. Elastic constants and pressure-induced phase transitions for Si and Ge, equilibrium structures, lattice parameters, bond lengths, and excess energies of Si-Ge superlattices are correctly predicted by our potential. We summarize our main conclusions as follows.

(i) The new Si and Ge interatomic potential give good

TABLE IV. Interplanar distances R, axial ratio c/a, and relaxation parameter ϵ for epitaxial Si_2Ge_2 superlattice grown pseudomorphically on a (001) oriented substrate with lattice parameters of Si (a_{Si}), Ge (a_{Ge}), and average of Si and Ge ($\bar{a}$). The values in parentheses are the calculated results obtained in valence-force-field geometry optimization using *ab initio* force constants (Ref. 38). Interplanar distances are in units of Å.

a_{sub}	R(Si—Si)	R(Si—Ge)	R(Ge—Ge)	c/a	ϵ_{Si}	ϵ_{Ge}
a_{Si}	1.3566	1.4026	1.4482	1.0337	−0.0327	0.0327
	(1.3488)	(1.3926)	(1.4378)	(1.0300)	(−0.0317)	(0.0322)
$\bar{a}$	1.3383	1.3821	1.4262	1.0000	−0.0318	0.0319
	(1.3303)	(1.3750)	(1.4220)	(0.9986)	(−0.0329)	(0.0337)
a_{Ge}	1.3207	1.3636	1.4078	0.9691	−0.0318	0.0321
	(1.3112)	(1.3568)	(1.4057)	(0.9680)	(−0.0342)	(0.0354)

estimates of the various elastic constants and their pressure derivatives.

(ii) The new interatomic potentials for Si and Ge reasonably reproduce the three stable and metastable states such as those with diamond, β-Sn(I), and β-Sn(II) structures in the energy calculations as a function of axial ratio. The calculated pressure-volume relationship for Si and Ge are in good agreement with experimental results in these with diamond and β-Sn structures. The relative stabilities among three states are reasonably predicted at the phase transition volume. These results suggest that the new potentials are suitable for the energetic study of the isotropic and tetragonal deformations, which are important in binary systems.

(iii) Equilibrium states of Si-Ge superlattices using Si, Ge, and Si-Ge interatomic potentials agree with experimental results. The calculated lattice parameters conform to the Vegard's law. The calculated bond lengths reproduce the expected bimodal distribution. The concentration dependence of the excess energies agrees well with the regular solution model. The calculated interplanar distance for the superlattice grown pseudomorphically on (001)-oriented substrate agree well with the results by first-principles calculation.

We conclude that these empirical interatomic potentials can be applied to Si-Ge binary systems. We are currently in the process of applying these potentials to the molecular-dynamics calculation of Si-Ge superlattice stabilities.

ACKNOWLEDGMENTS

The work was supported by the U.S. Office of Naval Research and U.S. Department of Defense. The authors are grateful to the University of Maryland Computing Center for use of the facilities.

[1]B. P. Feuston, R. K. Kalia, and P. Vashishta, Phys. Rev. B **35**, 6222 (1987).
[2]J. R. Chelikowsky, J. C. Phillips, M. Kawal, and M. Strauss, Phys. Rev. Lett. **62**, 292 (1989).
[3]R. Biswas, G. S. Grest, and C. M. Soukoulis, Phys. Rev. B **36**, 7437 (1987).
[4]M. D. Kluge and J. R. Ray, Phys. Rev. B **37**, 4132 (1988).
[5]B. W. Dodson, Phys. Rev. B **36**, 1068 (1987).
[6]M. Schneider, I. K. Schuller, and A. Rahman, Phys. Rev. B **36**, 1340 (1987).
[7]K. E. Khor and S. Das Sarma, Phys. Rev. B **36**, 7733 (1987).
[8]K. E. Khor and S. Das Sarma, Phys. Rev. B **38**, 3318 (1988).
[9]K. E. Khor and S. Das Sarma, Phys. Rev. B **39**, 1188 (1989).
[10]K. E. Khor and S. Das Sarma, Phys. Rev. B **40**, 1319 (1989).
[11]E. R. Cowley, Phys. Rev. Lett. **60**, 2379 (1988).
[12]F. H. Stillinger and T. A. Weber, Phys. Rev. B **31**, 5262 (1985).
[13]J. Tersoff, Phys. Rev. Lett. **56**, 632 (1986).
[14]R. Biswas and D. R. Hamann, Phys. Rev. Lett. **55**, 2001 (1985).
[15]D. C. Wallace, Rev. Mod. Phys. **37**, 57 (1965).
[16]T. Suzuki, A. V. Granato, and J. F. Thomas, Phys. Rev. **175**, 766 (1968).
[17]P. N. Keating, Phys. Rev. **145**, 637 (1966).
[18]R. M. Martin, Phys. Rev. B **1**, 4005 (1970).
[19]W. A. Harrison, *Electronic Structure and the Properties of Solids* (Freeman, New York, 1980).
[20]H. J. McSkimin and P. Andreatch, J. Appl. Phys. **34**, 651 (1963); **35**, 2161 (1964).
[21]R. Tubino, L. Piseri, and G. Zerbi, J. Chem. Phys. **56**, 1022 (1972).
[22]S. Minomura *et al.*, J. Non-Cryst. Solids **59&60**, 541 (1983).
[23]J. C. Bean, Science **230**, 127 (1985).
[24]S. Minomura and H. G. Drickamer, J. Phys. Chem. Solids **23**, 451 (1962).
[25]H. G. Drickamer, Rev. Sci. Instrum. **41**, 1667 (1970).
[26]J. C. Jamieson, Science **139**, 762 (1963); **139**, 845 (1963). Please note that the axial ratio (c/a) used in this study is different from the axial ratio $(c/a)_{\text{tetragonal}}$, where the body-centered-tetragonal lattice is taken as a unit cell. The axial ratio $(c/a)_{\text{tetragonal}}$ is converted as $\sqrt{2}(c/a)$.
[27]B. W. Dodson, Phys. Rev. B **35**, 2795 (1987).
[28]J. Tersoff, Phys. Rev. B **37**, 6991 (1988).
[29]M. Senoo, H. Mii, and I. Fujishiro, J. Phys. Soc. Jpn. **41**, 1562 (1976).
[30]J. Z. Hu and I. L. Spain, Solid State Commun. **51**, 263 (1984).
[31]R. People, IEEE J. Quantum Electron. **QE-22**, 1696 (1986).
[32]J. L. Martins and A. Zunger, Phys. Rev. Lett. **56**, 1400 (1986).
[33]A. Qteisch and R. Resta, Phys. Rev. B **37**, 1308 (1988).
[34]S. Ciraci and I. P. Batra, Phys. Rev. B **38**, 1835 (1988).
[35]J. P. Dismukes, L. Ekstrom, and R. J. Paff, J. Phys. Chem. **68**, 3021 (1964).
[36]G. P. Srivastava, J. L. Martins, and A. Zunger, Phys. Rev. B **31**, 2561 (1985).
[37]P. Boguslawski and A. Baldereschi, Solid State Commun. **66**, 679 (1988).
[38]S. Froyen, D. M. Wood, and A. Zunger, Phys. Rev. B **37**, 6893 (1988).